Journal Homepage: - www.journalijar.com

INTERNATIONAL JOURNAL OF ADVANCED RESEARCH (IJAR)

Article DOI: 10.21474/IJAR01/17089
DOI URL: http://dx.doi.org/10.21474/IJAR01/17089

RESEARCH ARTICLE

INVESTIGATION ON THE CRYSTALLINITY AND OPTOELECTRONIC PROPERTIES OF THIN FILMS OF ZnO/MAPbX$_3$HETEROJUNCTIONSYNTHESIZED VIA THE SPIN-COATING METHOD

Donafologo Soro[1], Klègayéré Emmanuel Koné[2], Amal Bouich[2,3], Júlia Marí-Guaita[2] and Bernabé Mari Soucase[2]

1. Département des Sciences et Technologie Ecole Normale Supérieure (ENS) d'Abidjan Côte d'Ivoire.
2. Department 1Institut de Disseny per a la Fabricació i Producció Automatitzada, Universitat Politècnica de València.
3. Fisica Aplicada a las Ingenierias Aeronautica y Naval & Instituto de Energia Solar, Universidad Politécnica de Madrid, Spain.

Manuscript Info

Manuscript History
Received: 15 April 2023
Final Accepted: 19 May 2023
Published: June 2023

Key words:-
ZnO/MAPbX$_3$, Optical Properties, Spin Coating, Surface Topography, Crystallinity

Abstract

In this paper, thin layers of ZnO were deposited onto fluorine-doped tin oxide (FTO) substrates. Subsequently, different layers of perovskite (MAPbX$_3$, X = I, Br, Cl) were spin-coated onto these ZnO layers. The resulting layers were characterized using X-ray diffraction (XRD), UV-Visible spectroscopy, and scanning electron microscopy (SEM). Special attention was given to the surface topography, the crystallinityand optoelectronic properties.XRD analysis of all the thin layers showed two diffraction peaks for the ZnO/MAPbX$_3$ heterojunction corresponding to the crystallographic planes (100) and (200). The ZnO/MAPbBr$_3$ peaks were more intense than the peaks from the ZnO/MAPbI$_3$ and ZnO/MAPbCl$_3$ samples. SEM images showed the crystalline nature of the produced thin layers. The grain size of the ZnO/MAPbBr$_3$ sample was approximately 747.00 nm, while those of the ZnO/MAPbI$_3$ and ZnO/MAPbCl$_3$ samples were 412.00 nm and 330.55 nm, respectively. UV-visible characterization demonstrated that the iodine-based sample had the highest solar radiation absorption and had the smallest bandgap, with Eg = 1.95 eV.

Introduction:-

In the field of photovoltaics, the first materials used were silicon, followed by Copper Indium Gallium Sulfur (CIGS) and CdTe organic cells, which belong to the second generation [1-3]. However, in recent years, the photovoltaic energy domain has witnessed the discovery of a new potential material for its development, known as the third generation—perovskite. Perovskites have the formula ABX$_3$ (where A = MA, FA, Cs; B = Pb, In, Sn; and X = Br, Cl, I), and this structure is highly versatile. Thin films of methylammonium lead halides (MaPbX$_3$) have emerged as promising materials in the field of photovoltaics. Their advent has sparked considerable interest due to their exceptional optoelectronic properties. These properties arise from the perovskite crystal structure, where organic cations such as methylammonium (MA^+) are combined with lead (Pb^{2+}) and halide (X^-) ions. This composition allows for efficient light absorption and charge carrier generation, thereby improving performance. Several methods are used to synthesize thin perovskite films, including vacuum deposition [4], solution-assisted vapor treatment [5], atomic layer deposition [6], one- and two-step solution processing [7,8], and spin coating [9].

Corresponding Author:- Donafologo Soro
Address**:-** Département des Sciences et Technologie Ecole Normale Supérieure (ENS) d'Abidjan Côte d'Ivoire.

Solution-based spin coating has become a versatile and scalable technique for depositing thin $MaPbX_3$ films, making them suitable for large-scale production. These deposition methods are rapid, simple, and cost-effective. Perovskites are therefore versatile semiconductors that combine high performance, low cost, and low-temperature processing capability for various applications such as photovoltaics and light emission. They have gained popularity due to these advantages [10-14], making them attractive. One of the key advantages of $MaPbX_3$ thin films is their tunable bandgap, allowing them to absorb a broad range of solar radiation, including visible and near-infrared light. This feature enables efficient utilization of the solar spectrum, leading to high photocurrent generation. Moreover, $MaPbX_3$ materials exhibit long charge carrier diffusion lengths, minimizing carrier recombination losses and improving charge collection efficiency.Despite their promising attributes, successful implementation of $MaPbX_3$ thin films in photovoltaic devices faces several challenges. These include stability issues, such as sensitivity to moisture and degradation upon prolonged exposure to light and heat. Extensive research efforts are focused on improving the stability and long-term performance of $MaPbX_3$ thin films to ensure their practical applicability under real conditions. Another point of interest would be analyzing surface topography, the crystallinity and determining their influence on the optoelectronic properties of these films. In this context, this comparative analysis aims to study the influence of surface topography and the crystallinity on the optoelectronic properties of thin films comprising various lead halide and methylammonium combinations, synthesized using the spin coating method. By examining the morphology, the crystallinity and optoelectronic characteristics of these films, we can better understand their suitability for photovoltaic applications and identify potential avenues for improvement. This study will provide insights into the advantages and disadvantages of these three materials ($MAPbI_3$, $MAPbBr_3$, $MAPbCl_3$) deposited on zinc oxide (ZnO). It should be noted that zinc oxide is a transparent conductive material with a wide direct bandgap of 3.3 eV [15]. This n-type oxide facilitates electron transport in the solar cell. Various deposition methods, including printing [16], inkjet [17], spray, dip-coating, spin-coating [18], are used to deposit the layers. Overall, the exploration of MaPbX3 thin films in the field of photovoltaics holds great promise for achieving efficient, cost-effective, and scalable solar energy conversion. Comparative analysis of surface topography and optoelectronic properties of these thin films can contribute to the development of enhanced materials and the advancement of next-generation solar cell technologies.

Experimental procedure

The 0.5 M zinc oxide (ZnO) solution was prepared by dissolving zinc acetate [$Zn(CH3COO)_2$, $2H_2O$] in ethanol. This prepared solution was spin-coated onto FTO glass substrates at a speed of 5000 rpm for 30 s. The resulting thin ZnO films were annealed at 450ºC and subsequently characterized. Prior to deposition, the FTO substrates were cleaned using deionized soapy water and placed in an ultrasonic bath for 5 minutes. Afterwards, the substrates were thoroughly rinsed with deionized water and different solvents in the following sequence: acetone and 2-propanol, each heated in an ultrasonic bath for 5 minutes. The ZnO thin films were then used for the deposition of perovskite layers using the same procedure and conditions.

For the deposition of the perovskite layers, three perovskite solutions ($MAPbX_3$, X = I, Br, Cl) were also prepared. Lead halide precursors (PbX_2) and methylammonium halide (MAX) were used to prepare the solution. Iodide-based precursors were dissolved in N,N-dimethylformamide (DMF), while bromide and chloride-based precursors were dissolved in dimethyl sulfoxide (DMSO). For the perovskite depositions, a few drops of ether were added only a few seconds after the rotation started. The added ether facilitated solvent evaporation, resulting in good morphology and crystallinity of the samples. The prepared films were characterized. The absorption and transmission of the samples were measured in the wavelength range of 300 to 900 nm using an Ocean Optic HR4000 spectrometer. The samples were characterized by X-ray diffraction using the RIGAKU Ultima IV diffractometer. The Scanning Field Emission Electron Microscope (FESEM) instrument was used to examine the surface morphology under a voltage of 1.5 kV.

Results and Discussion:-

The $ZnO/MAPbX_3$ heterojunction and the ZnO layer were characterized using X-ray diffraction (XRD), and the results are shown in Figure 1a. In this figure, two diffraction peaks from the ZnO layer were observed at $2\theta = 33.57º$ and $2\theta = 37.61º$, corresponding to the (002) and (101) planes of the hexagonal wurtzite structure (JCPDS Card No. 00-036-1451). From these XRD patterns, we can confirm that the ZnO thin films are polycrystalline. Figure 1a shows two diffraction peaks from the $ZnO/MAPbX_3$ heterojunction, corresponding to the (100) and (200) crystallographic planes. These peaks align well with those reported in the literature [19]. The $ZnO/MAPbI_3$ peaks were observed at $2\theta = 12.66º$ and $2\theta = 28.3º$ for the (002) and (101) planes, respectively, while those of $ZnO/MAPbCl_3$ were located at $2\theta = 11.05º$ and $2\theta = 32.23º$, respectively.The $ZnO/MAPbBr_3$ peaks were more intense and situated at $2\theta = 14.96º$ and $2\theta = 30.13º$ for the (002) and (101) planes, respectively. The height of peaks

in an X-ray diffraction spectrum is generally proportional to the X-ray scattering intensity from the crystalline planes of the material. Greater scattering intensity occurs when the crystalline planes are well-aligned and present over a larger distance, indicating higher regularity and structural order in the material, which corresponds to higher crystallinity. Therefore, higher crystallinity often results in more intense peaks in an X-ray diffraction spectrum. Consequently, the height of peaks can serve as an approximate indicator of the crystallinity of a material. Based on this analysis, we can conclude that the $ZnO/MAPbBr_3$ thin films exhibit good crystallinity compared to the $ZnO/MAPbI_3$ and $ZnO/MAPbCl_3$ thin films. However, it is important to note that other factors such as crystal size, the presence of defects, or impurities can also influence the observed peak heights.

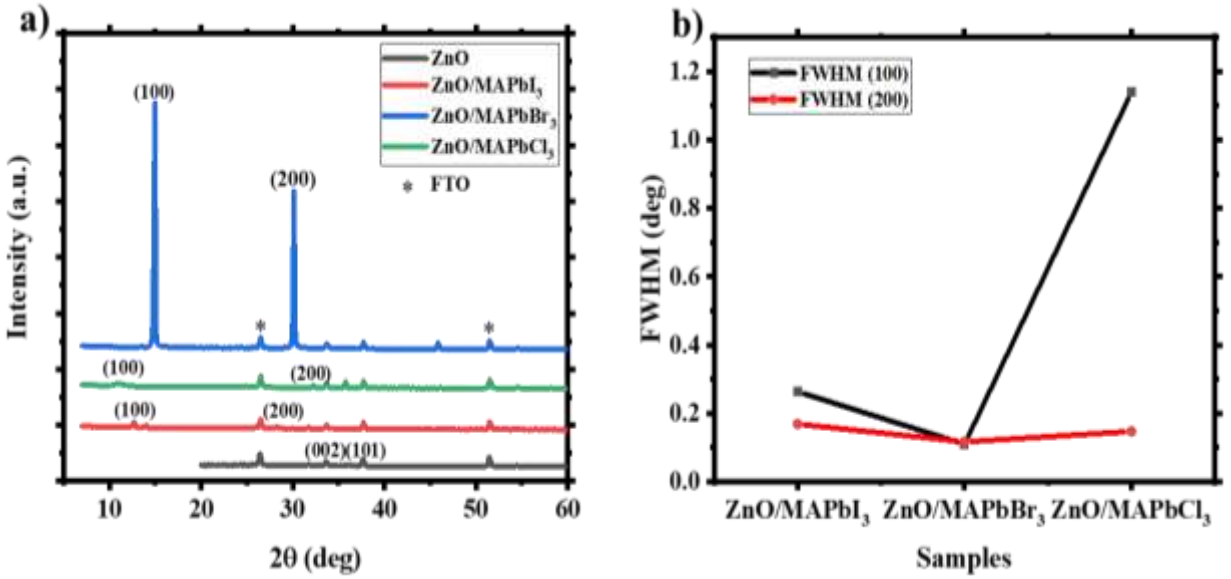

Figure 1:- a) XRD patterns of ZnO , $ZnO/MAPbI_3$, ZnO/MAPbBr3 and $ZnO/MAPbCl_3$
b) FWHM of samples products and for the crystallographic planes (100) and (200).

Crystal lattice effective strain was determined in order to know the grains defects and strains in the thin films using equation (1) [20,21].

$$\beta\cos(\theta) = \frac{\lambda k}{D} + 4\varepsilon\sin(\theta) \quad (1)$$

Where β : FWHM; k =0.94;
θ : Bragg angle;
D : grain size, and
λ = 0.1540 nm: the wavelength of the X-ray.
The curves of the maximum width at half maximum (FWHM) of the films products and for the crystallographic planes (100) and (200) are represented in figure 1b.
The equation (2) was used to calculate the lattice dislocation density [22]:

$$\delta = \frac{1}{D^2} \quad (2)$$

Grains size D were given by XRD results.

Results of different parameters calculated are summarized in **Table 1** . The bromine-based sample has the largest grain size of 747 nm. In general, when the grains are larger, there are fewer grain boundaries and defects in the material, which improves structural order and a more continuous crystal lattice. This leads to improved crystallinity and better overall thin film quality. These results confirm the good crystallinity of the samples $ZnO/MAPbBr_3$.

Table 1:- Parameters of XRD spectra of ZnO and ZnO/MAPbX3 films.

Samples ID	Grains size D (nm)	Dislocation density δ (nm^{-2})	Lattice strain ε
ZnO	401	$6.22x10^{-6}$	0.173
$ZnO/MAPbI_3$	412	$5.89x10^{-6}$	0.382
$ZnO/MAPbBr_3$	747	$1.79x10^{-6}$	0.159

$ZnO/MAPbCl_3$	330.55	$9.15x10^{-6}$	0.245

Figure 2 illustrates the absorption spectra of the different samples: $ZnO/MAPbI_3$, $ZnO/MAPbBr_3$, $ZnO/MAPbCl_3$, and ZnO. The $ZnO/MAPbI_3$ sample exhibits the highest absorption coefficient, approaching 1.5. This implies that it absorbs a significant amount of light across the entire measured wavelength range (300 nm to 900 nm). The absorption coefficients of the $ZnO/MAPbBr_3$ and $ZnO/MAPbCl_3$ samples range between 0.5 and 1, indicating moderate light absorption. Conversely, the absorption coefficient of the ZnO sample is less than 0.5 suggesting relatively weak light absorption. The discrepancy in the absorption coefficients can be attributed to the light or dark coloring of the different thin layers.in absorption coefficients can be attributed to the lightness or darkness of the different thin layers. In general, darker colors tend to have higher absorption coefficients, as they absorb more light. The $ZnO/MAPbI_3$ sample, which is iodine-based, tends to have a darker shade compared to the other samples, thus explaining its elevated absorption coefficient. Another factor contributing to the higher absorption of the $ZnO/MAPbI_3$ sample is its grain size. The grain size of $ZnO/MAPbI_3$ is measured to be 412 nm, while $ZnO/MAPbBr_3$ has a larger grain size of 747 nm. Smaller grains promote multiple scattering of incident wave energy. When waves encounter numerous small grains, they interact with a greater amount of material, resulting in increased absorption. Consequently, despite $ZnO/MAPbBr_3$ having superior crystallinity compared to $ZnO/MAPbI_3$, its absorption is lower

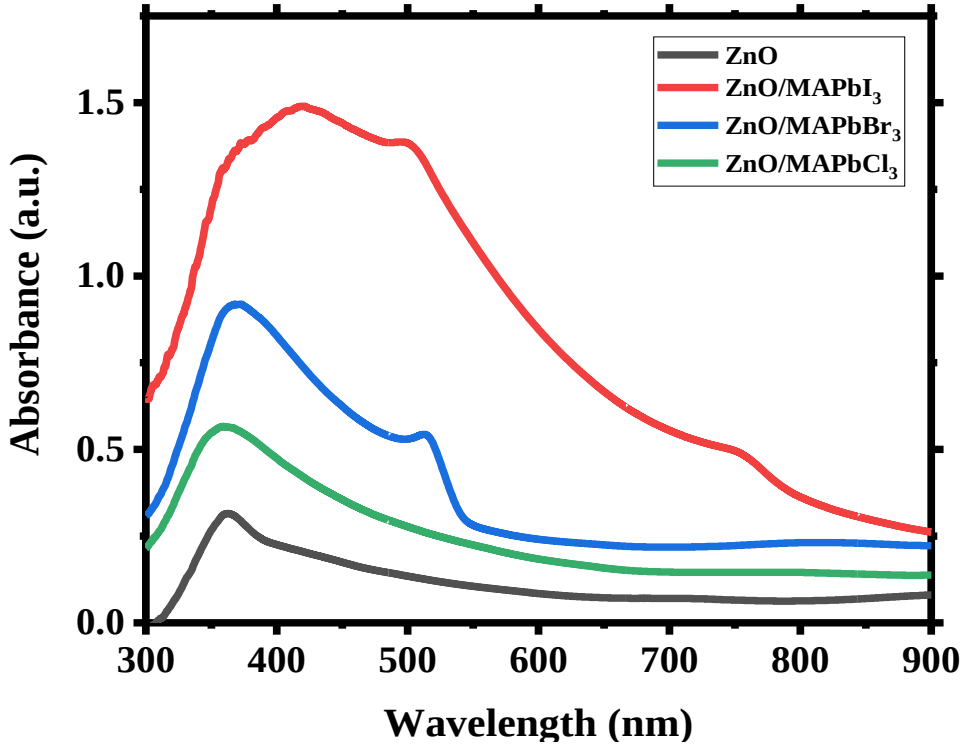

Figure 2:- UV–vis **absorption spectra of ZnO,$ZnO/MAPbI_3$,$ZnO/MAPbBr_3$ and $ZnO/MAPbCl_3$**

The passage explains the transmittance characteristics of the samples shown in **Figure 3**. Transmittance refers to the ability of a material to allow light to pass through it without significant absorption. According to the passage, the ZnO thin layers exhibit the highest transmittance among the samples, reaching approximately 80%. This means that around 80% of the incident light in the measured wavelength range is transmitted through the ZnO thin layers without being absorbed significantly. In other words, the ZnO thin layers allow a large portion of light to pass through them. On the other hand, the transmittance of the other samples ($ZnO/MAPbI_3$, $ZnO/MAPbBr_3$, and $ZnO/MAPbCl_3$) is lower, measuring below 60%. This suggests that these samples absorb a larger fraction of the incident light compared to the ZnO thin layers. As a result, less light is transmitted through these samples, resulting in lower transmittance values. The inverse relationship between transmittance and absorption is observed, as mentioned in previous passage. While the ZnO thin layers have high transmittance and low absorption, the other samples have lower transmittance and higher absorption coefficients, as described in the previous discussion.

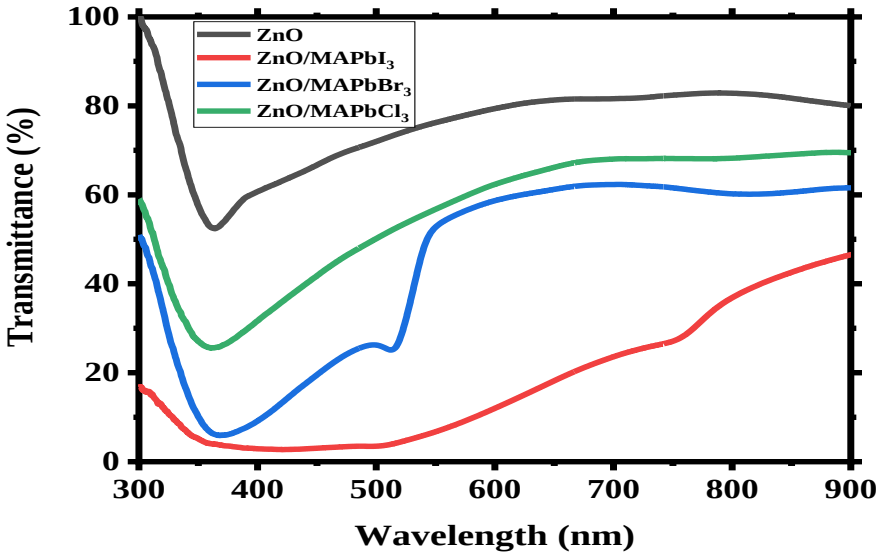

Figure 3:- Transmittance of ZnO,ZnO/$MAPbI_3$,ZnO/$MAPbBr_3$and ZnO/$MAPbCl_3$

The band gaps, represented in **Figure 4**, were determined based on the absorption data. The Tauc equation is used to calculate these values [23].

$(\alpha h\nu)^2 = \beta\,(h\nu - Eg)$ (3)

In this equation, β is a constant independent of the energy hν and α is the absorption coefficient. The bandgap values of the samples are summarized in **Table 2** . The band gap of ZnO is equal to 3.25 eV,which closely matches the value reported in the literature (3.3 eV) [24]. The band gaps of heterojunction thin films range from 1.95 eV to 2.7 eV.

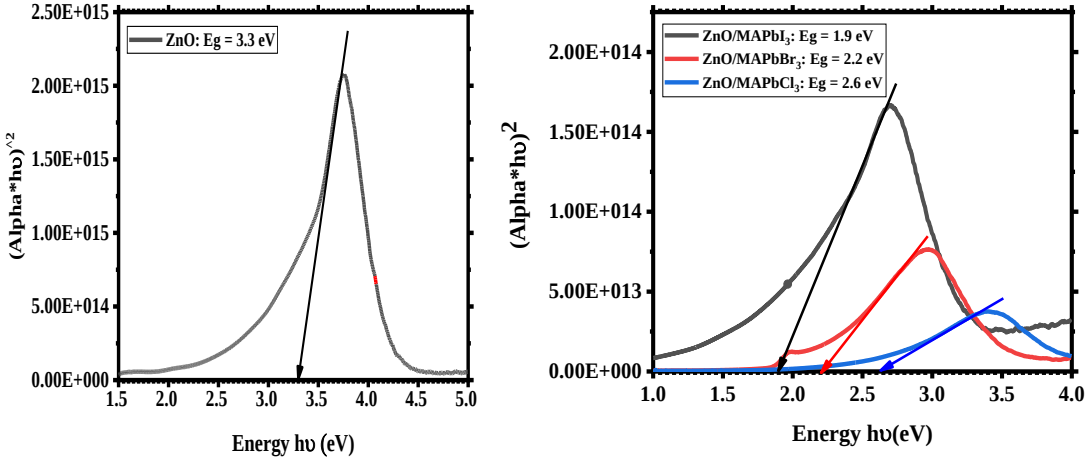

Figure 4:- Band gap of ZnO,ZnO/$MAPbI_3$,ZnO/$MAPbBr_3$and ZnO/$MAPbCl_3$

Table 2:- Band gaps of different samples.

Samples ID	Wavelength (nm)	Eg (eV)
ZnO	381	3.25
ZnO/$MAPbI_3$	635	1.95
ZnO/$MAPbBr_3$	563	2.2
ZnO/$MAPbCl_3$	459	2.7

Scanning electron microscopy (SEM) images of the samples are shown in **Figure 5**. These images provide visual evidence of the crystalline nature of the elaborate thin films, which agrees well with results obtained from diffraction analysis of the x-rays. They highlight certain characteristics of the samples.All samples $MAPbX_3$ show a cauliflower like morphology with aggregates and adherent to the substrate. The deposited films seem to be rough and their structure is less uniform In particular, for the $ZnO/MAPbBr_3$ sample, the SEM image reveals that it has the largest grain size among the samples. This observation is consistent with grain size information obtained from X-ray diffraction (XRD) data, indicating consistency between the two characterization techniques. SEM images demonstrate also good distribution of perovskite material on the grain surface of ZnO. This implies that the perovskite layer is well dispersed and covers the ZnO grains, although the grains themselves may not be clearly visiblein SEM images.

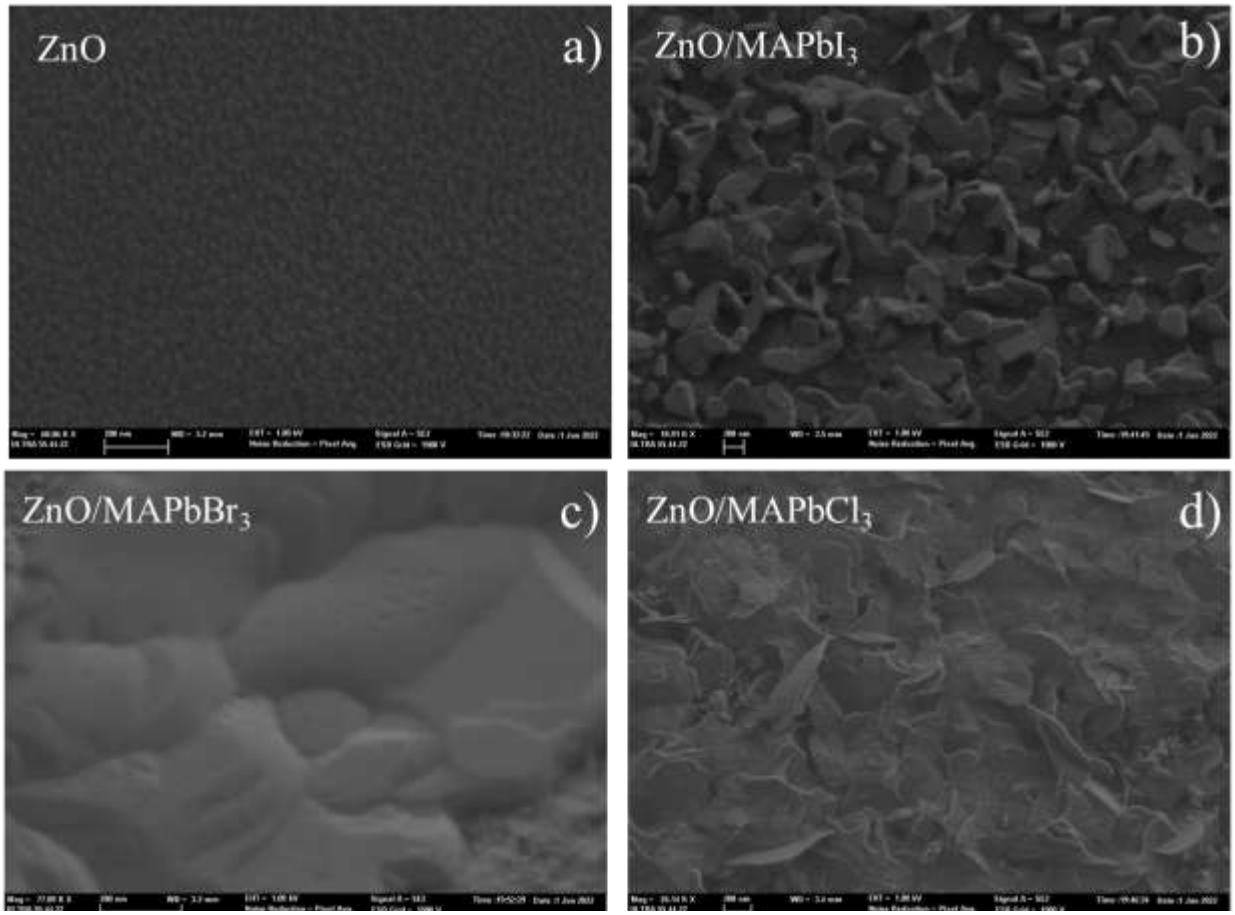

Figure 5:- SEM images of ZnO,$ZnO/MAPbI_3$,$ZnO/MAPbBr_3$and $ZnO/MAPbCl_3$

Conclusion:-

Thin layers of ZnO were deposited onto fluorine-doped tin oxide (FTO) substrates, followed by the deposition of distinct layers of $MaPbX_3$. X-ray diffraction (XRD) analysis of all the thin films revealed two diffraction peaks corresponding to the crystallographic planes (100) and (200) of the $ZnO/MAPbX_3$ heterojunction. All samples exhibited excellent crystal structure. The $ZnO/MAPbBr_3$ heterojunction displayed the most prominent diffraction peaks. The optoelectronic properties varied depending on the specific type of perovskite utilized. UV-visible characterization demonstrated that the iodine-based sample exhibited superior solar radiation absorption, with an absorption coefficient approaching 1.5. It also had the smallest band gap (Eg = 1.95 eV). The chlorine-based sample ($MAPbCl_3$) exhibited smaller grain sizes measuring 330.55 nm. Scanning electron microscopy (SEM) images confirmed the effective distribution of the perovskite material on the ZnO-coated substrates.

Acknowledgement:-
The authors acknowledge the support provided by Erasmus+ KA 107 which offers scholarships for the realization of this research..

Disclosure statement: **Conflict of Interest:**The authors declare that they have no known competing financial interests or personal relationships that could have appeared to influence the work reported in this paper.

References:-
[1] D. Soro, Y. Doumbia, M. Sidibé, B. Marí, S. Touré , M. Baneto. MAPb1 xInxBr3 perovskite crystals deposition and growth on fluorine doped tin oxide vol 18 (1), 41-53, June 2019.
[2] A. Bouich,., J. Marí-Guaita,., I. G .Pradas,., B. Marí,.. Towards manufacture stable lead perovskite APbI3 (A= Cs, MA, FA) based solar cells with low-cost techniques. Engineering Proceedings, 12 (1) 81. 1-5, January 2022.
[3] S..De Wolf, J..Holovsky, S. J Moon., P. Loper, , B .Niesen., M .Ledinsky, C. Ballif,. Organometallic halide perovskites: sharp optical absorption edge and its relation to photovoltaic performance. The journal of physical chemistry letters, 5(6), 1035-1039, March 2014.
[4]. M. Liu, M.B. Johnston, H.J, Efficient planar heterojunction perovskite solar cells by vapor deposition, Nature 501 (7467) , 395–398, September 2013.
[5] Q. Chen, H. Zhou, Z. Hong, S. Luo, H.S. Duan, H.H. Wang, Y. Liu, G. Li, Y. Yang. Planar hetero junction perovskite solar cells via vapor-assisted solution process J. Am. Chem. Soc, 136(2) 622–625, December 2013.
[6] B.R. Sutherland, S. Hoogland, M.M. Adachi, P. Kanjanaboos, C.T.O. Wong, J.J. McDowell, J. Xu, O. Voznyy, Z. Ning, A.J. Houtepen, E. Sargent,, Perovskite thin films via atomic layer deposition, Adv. Mater, 27 (1), 53–58,January 2015.
[7] J. Burschka, N. Pellet, S.J. Moon, R.H. Baker, P. Gao, M.K. Nazeeruddin, M. Gratzel, Sequential deposition as a route to high-Performance perovskite-Sensitized solar cells, Nature, 499 (7458), 316–319, July 2013.
[8] J.M. Ball, M.M. Lee, A. Hey, H.J. Snaith, Low-temperature processed meso-superstructured to thin-film perovskite solar cells,, Energy Environ. Sci. 6 (6), 1739–1743, Mar 2013.
[10] C-B. Juan Pablo, S. Michael., B. Tonio., G. Michael., A. Antonio., T., Wolfgang., and H., Anders. Promises and challenges of perovskite solar cells. Science,358 (6364), 739-744, November 2017.
[11] T. Nakada, S. Shirakata. Impacts of pulsed-laser assisted deposition on CIGS thin films and solar cells. Solar Energy Materials and Solar Cells, 95 (6),1463-1470, June 2011.
[12] F. Zhao, Y. Guo, J. Tao, Z. Li, J. Jiang, and Junhao. Investigation of CsPbBr3 films with controllable morphology and its influence on the photovoltaic properties for carbon-based planar perovskite solar cells. Applied Optics ,59 (18) 5481-5486, June 2020.
[13] H. Mehd. A. Mhamdi. R. and A. Bouazizi Hannachib, MAPbBr3 perovskite solar cells via a two-step deposition process . RSC Advances; 9 (23), 12906-12912, April 2019.
[14] S. Jin, Y. Wei, F. Huang, X. Yang, D. Luo, Y. Fang and J. Wu, J. Enhancing the perovskite solar cell performance by the treatment with mixed anti-solventJournal of Power Sources ,404(15), 64-72, November 2018.
[15] , S .Gledhill., A.Grimm, , N .Allsop,., T.Koehler, , C.Camus, , M..Lux-Steiner, C. H. Fischer,A spray pyrolysis route to the undoped ZnO layer of Cu (In, Ga)(S, Se)2 solar cells. Thin Solid Films, 517(7), 2309-2311, February 2009.
[16] T. M .Schmidt,Larsen,T. T Olsen, J. E., Carlé, D. Angmo, F .Krebs,. CUpscaling of perovskite solar cells: fully ambient roll processing of flexible perovskite solar cells with printed back electrodes. Advanced Energy Materials, 5(15), 1500569, June 2015.
[17] H.Zhou, , Q.Chen, , G.Li, , S.Luo, T. B Song, H. S .Duan,., Y .Yang,. Interface engineering of highly efficient perovskite solar cells. Science, 345(6196), 542-546, August 2014.
[18] M. C .Tang, H. X.Dang, S., Lee, D.Barrit, , R. Munir., , K.Wang, A. Amassian,. Wide and Tunable Bandgap MAPbBr3− xClx Hybrid Perovskites with Enhanced Phase Stability: In Situ Investigation and Photovoltaic Devices. Solar RRL, 5(4), 2000718, February 2021.
[19] Q. Chen, N. De Marco, M. Yang, B. Song, C. Chen, H. Zhao and Y. Yang, Under the spotlight: The organic–inorganic hybrid halide perovskite for optoelectronic applications Nano Today, 10 (3), 355–396, June 2015.
[20] S .Ullah,. , A .Bouich., H.,.Ullah, B.,.Mari,, M.Mollar, Enhanced optical and structural properties of V-doped binary SnS2 buffer layer. Solar Energy, 204, 654-659, July 2020.
[21] S.Ullah, A. Bouich, H. Ullah, B. Mari, M .Mollar, Comparative study of binary cadmium sulfide (CdS) and tin disulfide (SnS2) thin buffer layers. Solar Energy, 208, 637-642 ,September 2020.

[22] A..Bouich, , B .Hartiti, S.Ullah, H., Ullah, M Ebn Touhami,., D. M. F .Santos, B .Mari,. Optoelectronic characterization of CuInGa (S) 2 thin films grown by spray pyrolysis for photovoltaic application. Applied Physics A, 125(8), 1-9, August 2019.
[23] R..Sharma,, A. D .Acharya, S. B .Shrivastava, M. M. Patidar, M. Gangrade, T.Shripathi, V .Ganesan,. Studies on the structure optical and electrical properties of Zn-doped NiO thin films grown by spray pyrolysis. Optik, 127(11), 4661-4668, June 2016.
[24] Y. H .Hu, Y. J., Xie, M. H .Qu, , L. F.Wang, H. J. Xu,. Studying on the Preparation and Characteristics of Al2O3-Based Textured ZnO Thin Films. In 2010 Symposium on Photonics and Optoelectronics IEEE 1- 4, June.2010.